ACS OMEGA

Open Access

http://pubs.acs.org/journal/acsodf

Article

Origins of the Ediacaran Doushantuo High-Grade Primary Phosphorites at Kaiyang, Guizhou Province, China

Wenming Wu, Ruidong Yang,* Jianzhong Liu, Zepeng Wang, Shaohu Li, Yunbin Shao, Yamei Deng, Taiping Ye, Chaokun Luo, Lei Gao, Jiyan Chen, Haili Ren, Chengfu Yang, Junhai Li, Daxue Wan, and Wenxing Tai

Cite This: *ACS Omega* 2023, 8, 47938−47953

Read Online

ACCESS | Metrics & More | Article Recommendations

ABSTRACT: The Ediacaran Doushantuo phosphate deposit in Kaiyang, Guizhou Province, China, contains thick phosphate ores. Most of the ores are reconstituted phosphorite, and there have been few studies of the primary phosphorites, which has led to controversy regarding the origins and nature of mineralization of these phosphate-rich deposits. We identified high-grade primary phosphorites in the Kaiyang area and undertook a stratigraphic, petrological, sedimentological, geochemical, and isotopic study of these rocks. Moving up-section, the Longshui phosphate ore deposit comprises granular, micritic, stromatolitic, honeycomb, and sandy phosphorites. The first four types of phosphorite contain abundant biological structures, such as spherical, lobe-like, and amorphous forms. These are mainly fossils of benthic multicellular red algae, along with other types of algae. These fossils comprise >70% of the phosphorites, indicating that these are protist phosphorites. The ores are massive, unstratified, and contain numerous layered cavity structures, indicating that the ore bed was originally a reef. The phosphorites have P_2O_5 contents of 38.6−40.2 wt %, with an average of 38.9 wt %. The Al_2O_3 + TiO_2 values are 0.02−0.44 wt %. The $\delta^{18}O$ values of the samples vary from 13.76 to 16.57‰, with an average of 14.60‰, and $\delta^{13}C$ values range from −15.789 to −8.697‰, with an average of −13.133‰. The samples exhibit rare-earth element patterns that are enriched with middle rare-earth elements and have strongly negative Ce anomalies. The geochemical features show that the reef was deposited in clear and oxidized waters. The discovery of this high-grade protist phosphorite shows that the involvement of algae was key to the formation of the Kaiyang phosphate-rich deposit.

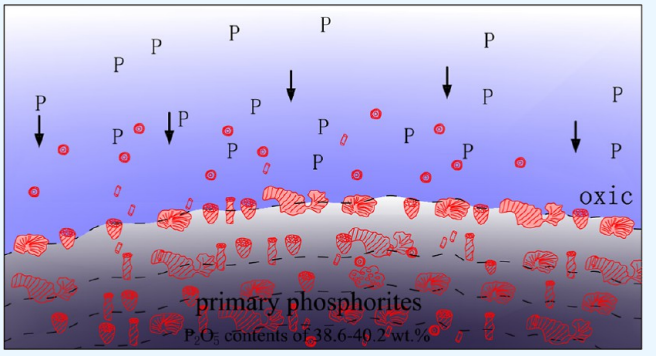

1. INTRODUCTION

The Kaiyang area in Guizhou Province contains a typical sedimentary phosphate deposit, which is of high grade and thick. As of 2017, the area had 15.3 billion tons of confirmed phosphate ore resources, with an average grade of >30 wt %, accounting for *d* ∼ 66% of China phosphate resources. Therefore, the ore-forming mechanisms of the Kaiyang superlarge phosphate deposit are an important area of research. The phosphate ore layer is in the Sinian (Ediacaran) Doushantuo Formation. The Doushantuo Formation is distinctly similar to these formations, which were deposited between 635.2 ± 0.6 and 551.1 ± 0.7 Ma.[1−3]

There is considerable controversy regarding the formation of the Doushantuo Formation phosphorites in Guizhou Province. The main hypotheses involve biomineralization,[4,5] inorganic precipitation, and physical enrichment.[6−8] Previous studies of phosphorite mineralization have focused mainly on its petrology and geochemistry. Interbedded phosphatic rocks,[4] microfossil assemblages,[9,10] algal fossils,[11−13] and animal embryo fossils[14] are widely distributed in the phosphorite ores, indicating that there was a relationship between phosphorite formation and biological processes. The phosphorites in the Weng'an and Kaiyang areas are enriched in elements involved in biological processes, such as Cr, Co, Pb, Ga, and Sr,[15,16] with Pb showing the most significant affinity for S. The rare-earth element patterns of phosphorites in this region exhibit slight enrichment in middle rare-earth elements, which is indicative of the role of microbes during mineralization.[10,17−20]

Previous studies of phosphate mineralization in the study area have focused mainly on reworked phosphatic conglom-

Received: August 30, 2023
Revised: November 22, 2023
Accepted: November 30, 2023
Published: December 6, 2023

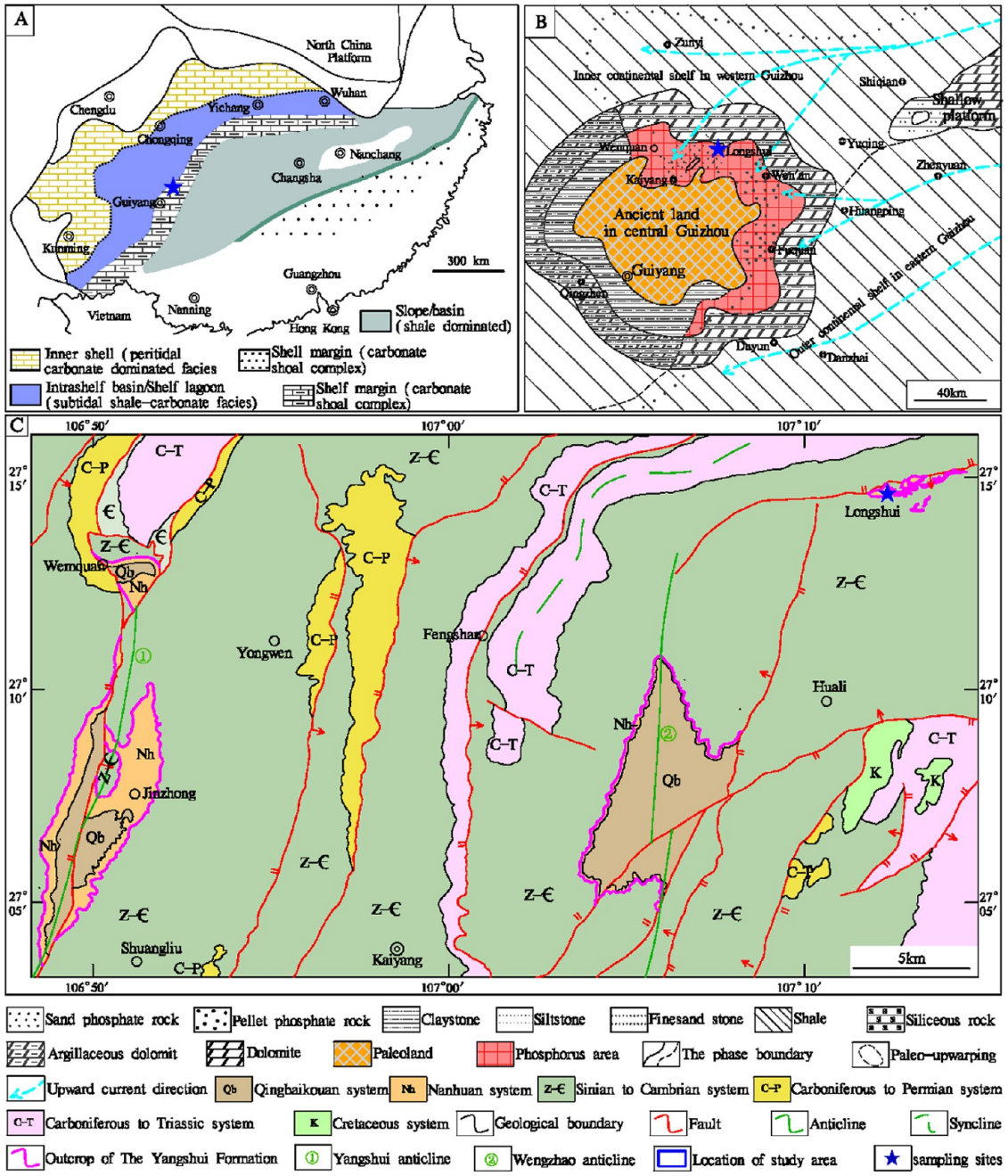

Figure 1. Regional geology of the study area. (A) Simplified map of China showing the location of the Yangtze Craton (yellow). Figure reproduced with permission from ref 24. Copyright 2011 Jiang et al. (B) Lithofacies and paleogeography in early and middle Ediacaran in central Guizhou. Figure reproduced with permission from ref 33. Copyright 2015 Chen et al. (C) Geological map of the Kaiyang area in the Guizhou Province.

erates.[7,21] Reworked phosphatic conglomerates are the main constituents of phosphate deposits in the Kaiyang region. They are the products of primary phosphatic conglomerates that have been broken, eroded, transported, and redeposited. As such, these rocks have undergone significant later modification. Therefore, in order to understand why large and high-grade phosphate deposits formed in the Kaiyang region, it is necessary to investigate primary phosphatic conglomerates. This study focused on a geological profile that contains a large number of primary phosphatic conglomerates. Samples from the profile were subjected to sedimentological, petrological, and geochemical investigations with the aim of constraining the ore-forming process and sedimentary depositional environments. These results allow an ore-forming model to be constructed for the superlarge and high-grade phosphate deposits in the study area.

2. GEOLOGICAL SETTING

2.1. Regional Geology. Due to breakup of the supercontinent Rodinia in the early Neoproterozoic, the Yangtze and Huaxia plates began to rift apart.[22,23] During the extensional stage, intense volcanism and seafloor hydrothermal activity accompanied the deposition of a continental–marine, volcanic–sedimentary rock system on the Yangtze Platform and in rift basins. The vast Yangtze Platform and rift basins in southern China also underwent glacial–interglacial sedimenta-

https://doi.org/10.1021/acsomega.3c06476
ACS Omega 2023, 8, 47938–47953

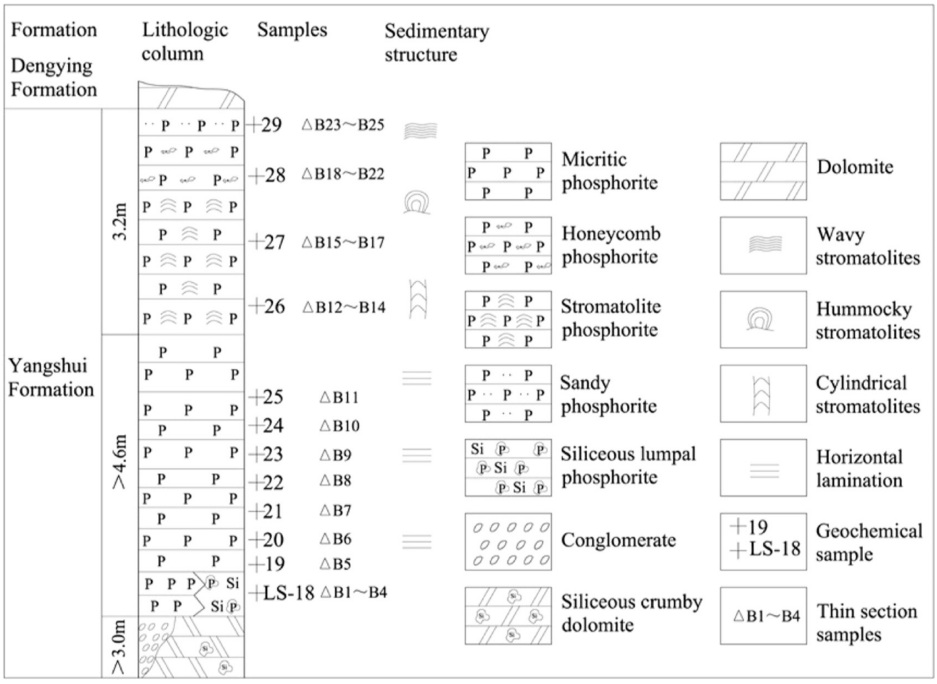

Figure 2. Stratigraphy of layer B at Longshui in the Kaiyang area.

tion during the Ediacaran, as a result of Snowball Earth. After the end of the global glaciation, the sedimentary basement of the Huaxia Plate had formed, and the southern China region had transitioned from a rift basin to a passive continental margin.[24,25] Volcanic activity decreased significantly, and the entire southern China paleo-continent began to experience continuous and stable marine sedimentation.[26] During the Cambrian, the Yangtze Platform was covered with a mixed sedimentary sequence of clastic, carbonate, and phosphatic rocks, which graded into a deep-water basin dominated by clastic and siliceous sedimentation to the southeast.[22,24,27−29] The study area is located on the southeastern margin of the Yangtze Platform. The Kaiyang area is situated on the northern edge of the ancient Guizhou continent of the Yangtze Block (Figure 2B) and was in a shallow-marine platform environment[30,31] with a moderate seawater depth during deposition of the Doushantuo Formation. The paleogeography controlled the formation and distribution of phosphate deposits in the Doushantuo Formation in central Guizhou. After the Marinoan glaciation, a marine transgression occurred in central Guizhou. Frequent marine transgressions occurred during the early depositional stages of the Doushantuo Formation. Gray and black−gray, thin-bedded phosphorites (layer A) were deposited in relatively low topographic parts of the Weng'an, Fuquan, and Kaiyang−Longshui areas. During deposition of the middle Doushantuo Formation, dolomites were deposited in these areas as the first period of phosphate-rich seawater came to an end. During the late depositional stages of the Doushantuo Formation, sea level continued to rise, and the second period of phosphate-rich seawater transgressed from the east to west to the Kaiyang−Shuangliu areas. Black and gray−black, clastic, banded, and dense phosphorites and dolomitic phosphorites (layer B) were then deposited.[32]

2.2. Geology of the Deposit. *2.2.1. Phosphorite Lithologies.* The Doushantuo Formation in the Longshui area (Figure 1C) consists of thin-bedded purple clay rocks, thin- to thick-bedded dark gray clastic phosphorites, thick-bedded gray−(white) siliceous dolomites, and dark gray micritic and stromatolitic phosphorites (layer B) (from base to top). The bottom of layer B comprises (dark) gray, thick-bedded phosphorites that contain siliceous nodules (near Zimeiyan; 107°13′20″E, 27°14′31″N). The lower and middle parts of layer B are dark gray, thick-bedded to massive, micritic phosphorites. The upper part comprises dark gray, cylindrical, mound-like, and wavy stromatolitic phosphorites and sandy phosphorites (near Dapingshan; 107°23′11″E, 27°14′05″) (Figure 2).

2.2.2. Sedimentary Features of Layer B. The thickness of layer B in the Longshui phosphate mine varies considerably (0−7.5 m). It has a basin-like form and occurs between siliceous conglomerates and other sedimentary rocks (Figure 3A,B). Its contact with the underlying strata is undulating, but contact with the overlying dolomite is relatively flat. From the base up, the ore deposit consists of phosphorite with siliceous nodules (Figure 3C), micritic phosphorite (Figure 3D), stromatolitic phosphorite (Figure 3F,G), honeycomb phosphorite (Figure 3H), and sandy phosphorite. The phosphorite with nodules is massive and unstratified. The nodules are white, nearly spherical to irregularly shaped (Figure 3C), and have diameters of 0.3−2.0 cm. The nodules are filled with silica, and quartz geodes occur locally. The micritic phosphorite is massive but has some localized bedding (Figure 3D) and contains a few stromatolites. The stromatolites are cylindrical, with upper convex structures (Figure 3F), wall structures (Figure 3G), and holes, and they do not contain lamina of light and dark interlayers (Figure 3F). Columns in the stromatolites are infilled with siliceous or phosphatic conglomerates that contain rounded and moderately sorted clasts. A large number of lamellar holes with diameters ranging from 0.2 to 40 mm (Figure 3H) are distributed in the honeycomb phosphorite, and the edges of these holes are curved. The sandy phosphorite is unstratified.

https://doi.org/10.1021/acsomega.3c06476
ACS Omega 2023, 8, 47938−47953

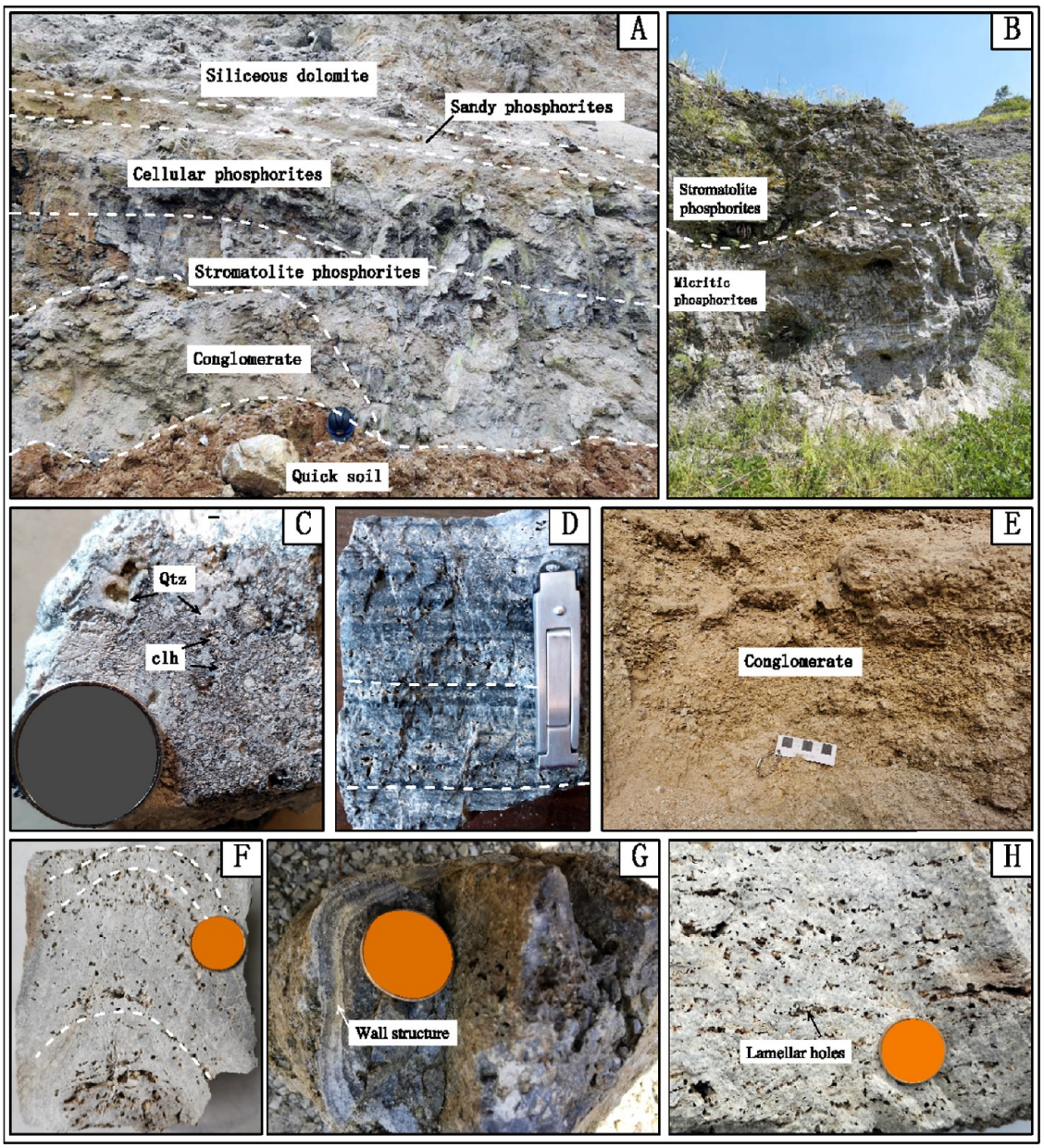

Figure 3. Sedimentary features of layer B at Longshui in the Kaiyang area: (A,B) phosphorite (Dapingshan, Longshui); (C) phosphorite with siliceous nodules (Zimeiyan, Longshui), the diameter of the iron sheet is 19 mm; (D) bedded micritic phosphorite (Dapingshan, Longshui), the long axis of the nail clipper is 60 mm; (E) conglomerate at the base of the ore bed; (F) longitudinal section of a columnar stromatolite with an upper convex structure (Dapingshan, Longshui); (G) cross-section of a columnar stromatolite with a wall structure (Dapingshan, Longshui); and (H) honeycomb phosphorite (Dapingshan, Longshui), the diameter of the iron sheet in F/G/H is 21 mm; clh = collophanite; Qtz = quartz.

3. SAMPLING AND ANALYTICAL METHODS

3.1. Sampling Sites. A total of 25 thin sections of samples of various types of phosphorite from layer B at Longshui were prepared, including four nodular phosphorites (samples B1−B4), seven micritic phosphorites (samples B5−B11), six stromatolitic phosphorites (samples B12−B17), five honeycomb phosphorites (samples B18−B22), and three wavy stromatolites (samples B23−B25) (Figure 2). Twelve samples for geochemical analysis were collected from layer B in the Doushantuo Formation (Figure 2), including one nodular phosphorite (sample LS18), seven micritic phosphorites (samples LS19−LS25), two stromatolitic phosphorites (LS26−LS27), one honeycomb phosphorite (LS28), and one sandy stromatolite (LS29). All samples were relatively unaltered.

3.2. Analytical Methods. Doubly polished thin sections were prepared by the Langfang Tuoxuan Rock Ore Detection Service Company Limited. The thin sections were examined using a Laika DM4500P polarizing microscope in the Guizhou Bureau of Geology and Mineral Resources, and microstructures were photographed.

The geochemical samples were sieved with 200 mm mesh prior to analysis, and parts of each sample were made into polished thin sections to examine the mineralogy, textures, and fossils. Whole-rock major and trace elements were analyzed at the ALS Minerals Company Limited, Guangzhou, China. Whole-rock stable C−O isotope analyses were conducted at

https://doi.org/10.1021/acsomega.3c06476
ACS Omega 2023, 8, 47938−47953

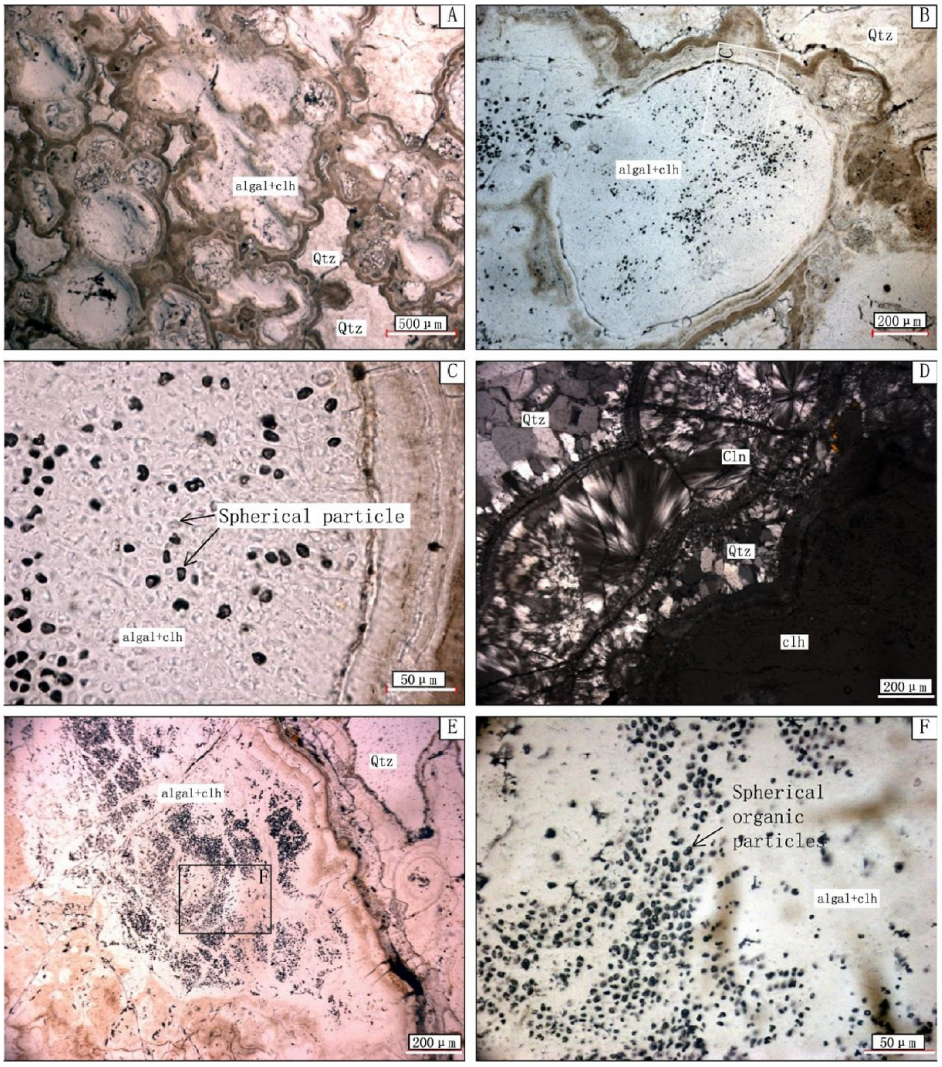

Figure 4. Microscopic characteristics of the spherulite-rich nodular phosphorite. (A−C) Nodular texture with rounded or irregular collophanite, which contains numerous dark gray or transparent spherical particles of organic matter. Quartz infills spaces between the aggregates (sample B1; Zimeiyan, Longshui). (D) Grainy structure with quartz and calcrete developed around the phosphatic aggregates (sample B2; Zimeiyan, Longshui). (E,F) Phosphatic aggregates containing numerous dark gray spherical particles of organic matter (sample B3; Zimeiyan, Longshui). clh = collophanite; Qtz = quartz; and Cln = chalcedony.

the Institute of Geographic Sciences and Natural Resources Research, CAS, Beijing, China.

The SiO_2, Al_2O_3, TiO_2, TFeO, MnO, CaO, MgO, K_2O, and P_2O_5 contents of the phosphorites were determined by X-ray fluorescence (the test method code is ME-XRF24) spectrometry. The wall rocks were also analyzed by X-ray fluorescence (XRF) spectrometry (the test method code is ME-XRF26). The phosphorite samples were digested in a $LiNO_3$ solution, and the wall rocks were mixed with $Li_2B_4O_7$ and fused at 950 °C. The loss-on-ignition (LOI) values were determined from the weight loss after heating to 950 °C. The detection limit for the major elements is 0.01 wt %, and the errors are < ± 3%.

Trace elements were analyzed by quadrupole inductively coupled plasma mass spectrometry (Q-ICP−MS; ELAN-DRC-e ICP−MS), with relative errors of < ± 10%. Aliquots (50 mg) of each sample were completely digested in a mixture of HF and HNO_3, and an internal standard was added (40 ng/mL Rh). The analytical methodology followed that of Qi et al. (2000). The detection limits were as follows: Tb, Ho, Lu, Cs, and Tm (0.01 ppm); Er, Eu, Sm, Pr, and Yb (0.03 ppm); Ba, Ce, Co, Th, Gd, Dy, and U (0.05 ppm); Rb, Cu, Ni, Nb, and Hf (0.2 ppm); Ta, Nd, Ga, and Sr (0.1 ppm); Y, Tl, Pb, and La (0.5 ppm); Zr and Mo (2 ppm); W and Sn (1 ppm); V (5 ppm); and Cr (10 ppm).

Stable C−O isotope ratios were measured by MS. Carbon in the samples was converted to CO_2 by combustion. Oxygen in the samples was converted to CO by high-temperature pyrolysis. CO_2 and CO were separated on a molecular sieve chromatographic column and then analyzed with a ConFlo interface access mass spectrometer. The internal precisions were <0.06‰ for $\delta^{13}C$ and <0.15‰ for $\delta^{18}O$. The external reproducibility was < ± 0.15‰.

4. RESULTS

4.1. Petrography. *4.1.1. Microstructures in the Nodular Phosphorites.* Fully matted phosphatic aggregates formed before the siliceous nodules in the nodular phosphorite (Figure 4A,D). Numerous unoriented spherical particles occur inside some of the phosphatic aggregates (Figure 4B,C), which are 10−15 μm in diameter, deflated in shape, translucent, and in

https://doi.org/10.1021/acsomega.3c06476
ACS Omega 2023, 8, 47938−47953

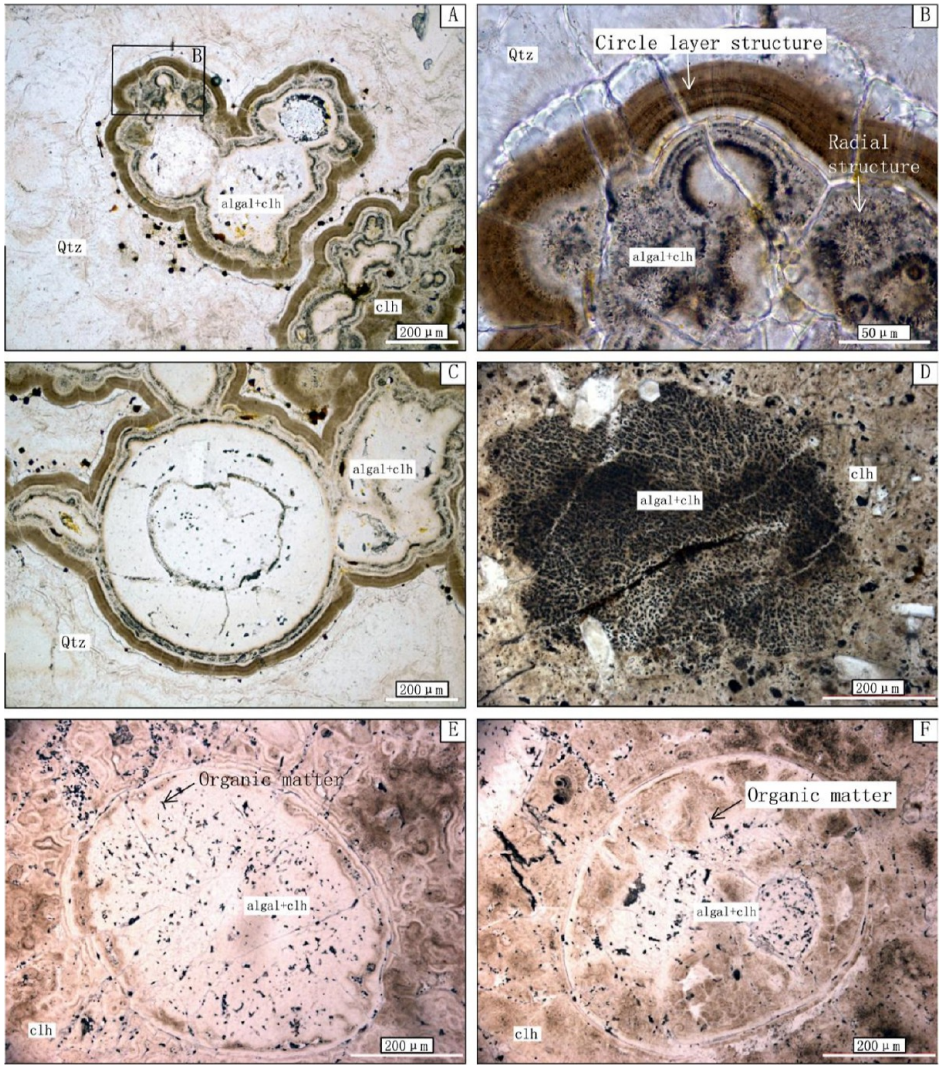

Figure 5. Microscopic features of the nodular phosphorite with a spherical structure. (A) Nodular structure (sample B1; Zimeiyan, Longshui). (B) Radial and concentric ring structure developed in phosphatic aggregates (sample B1; Zimeiyan, Longshui). (C) Concentric structure containing abundant aggregates of fine-grained particles (sample B1; Zimeiyan, Longshui). (D) Leaf-like structure comprising numerous oriented, dark gray particles of organic matter (sample B2; Zimeiyan, Longshui). (E) Spherical structure containing organic matter (sample B3; Zimeiyan, Longshui). (F) Spherical structure containing irregular organic matter and spherical particles (sample B3; Zimeiyan, Longshui). clh = collophanite; Qtz = quartz; Cln = chalcedony.

some cases dark. Light to dark layers occur at the margins of the aggregates (Figure 4B). The nodules are filled with silica, and quartz geodes are locally developed. Some of the nodules are coated with quartz or chalcedony (Figure 4D). Some of the phosphatic aggregates contain oriented spherical particles with diameters of <10 μm (Figure 4E,F). These aggregates have diameters of >2 mm. Some of the phosphatic aggregates have a cloud-like shape (Figure 5A) and diameters of >700 μm. There are multiple chambers in the aggregates, and the structures of each chamber are different. Leaf-like (Figure 5D) and spherical (Figure 5E,F) structures occur in some aggregates.

4.1.2. Microstructures in the Micritic, Stromatolitic, and Honeycomb Phosphorites. The micritic, stromatolitic, and honeycomb phosphorites have similar structures and thus are described together here. These rocks consist of >98% collophanite and <2% euhedral−subhedral quartz crystals. A large number of oriented and unoriented spherical particles occur in the collophanite. These particles are <10 μm in diameter and dark in color (Figure 6). The spherical particles may have concentric ring structures (Figure 6A) and contain granular (Figure 6B) and filamentous (Figure 6C,D) material along with granular bodies containing a large amount of organic matter (Figure 6E). The particles can be isolated or can occur in aggregates (Figure 6F). There are gourd-shaped, jellyfish-like, and bark-like structures.

4.2. Major Elements. The major element data for the phosphorites are listed in Table 1. The phosphorites consist mainly of P_2O_5, CaO, SiO_2, Al_2O_3, Fe_2O_3, and MgO. The nodular phosphorite (sample LS18) and stromatolitic phosphorite (sample LS29) have lower P_2O_5 contents (27.9 and 31.9 wt %, respectively) due to their high SiO_2 contents (27.10 and 16.56 wt %, respectively). These samples have CaO = 39.10 and 45.80 wt %, F = 3.00 and 3.30 wt %, Al_2O_3 < 0.01 wt % and = 0.03 wt %, K_2O = 0.01 wt %, and TiO_2 < 0.01 wt %.

The P_2O_5 contents of the samples LS20−LS28 vary from 38.60 to 40.20 wt % (Table 1; Figure 8), with an average of 38.94 wt %. CaO contents range from 53.40 to 54.10 wt %,

https://doi.org/10.1021/acsomega.3c06476
ACS Omega 2023, 8, 47938−47953

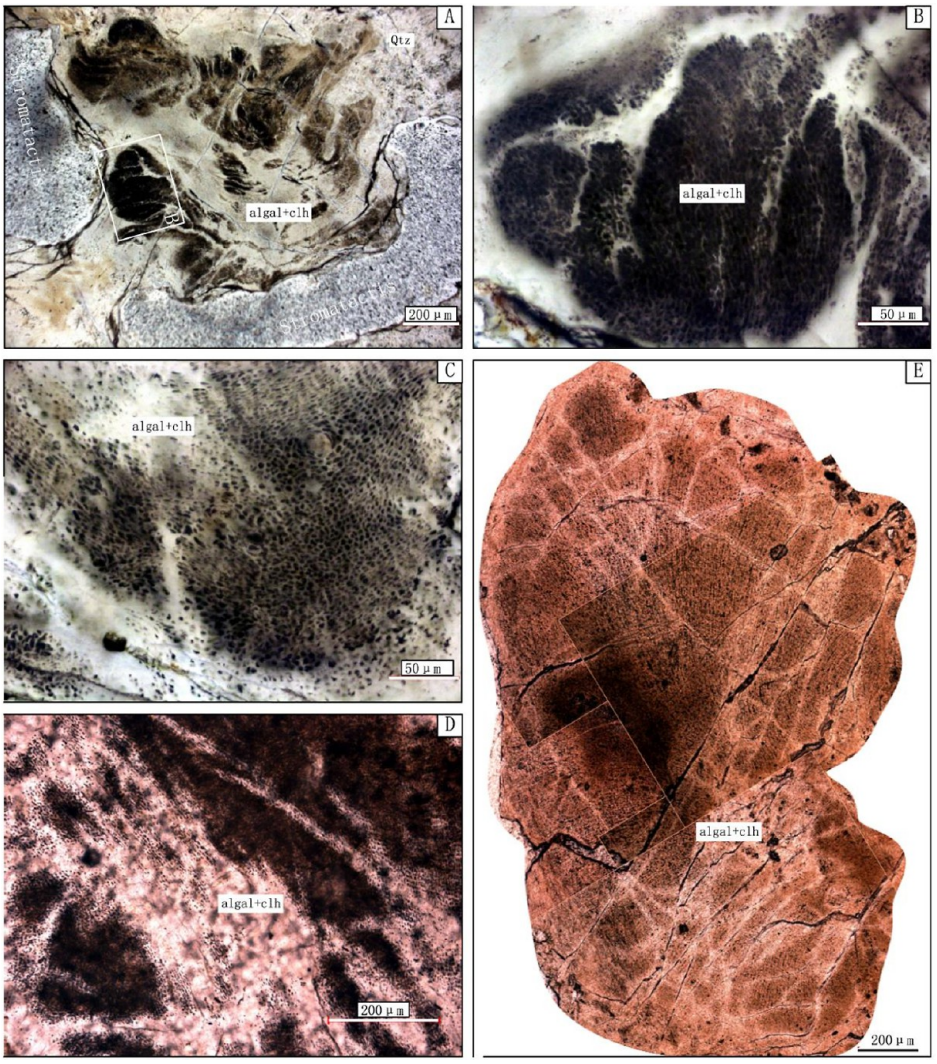

Figure 6. Microscopic characteristics of the micritic phosphorite. (A,B) Leaf-like structure comprising numerous oriented, dark gray, spherical particles of organic matter (sample B18; Dapingshan, Longshui). (C) Leaf-like structure comprising abundant oriented, dark gray, spherical particles of organic matter (sample B18; Dapingshan, Longshui). (D) Leaf-like structure comprising oriented, dark gray, spherical particles of organic matter in a circular stromatolite (sample B7; Dapingshan, Longshui). (E) Leaf-like structure comprising abundant irregular particles of organic matter in a radial pattern (sample B6; Dapingshan, Longshui). clh = collophanite; Qtz = quartz; Cln = chalcedony.

Table 1. Major Element Data (in wt %) for Phosphorites in Layer B

sampling sites	CaO	P_2O_5	F	SiO_2	TFe_2O_3	Al_2O_3	MgO	K_2O	Na_2O	TiO_2	LOI	CaO/P_2O_5	$Al_2O_3 + TiO_2$
LS-18	39.10	27.90	3.00	27.10	0.13	<0.01	0.63	0.01	0.23	<0.01	2.74	1.40	<0.02
LS-19	54.00	38.90	4.40	0.84	0.34	0.09	0.10	0.03	0.32	0.01	2.18	1.87	0.10
LS-20	53.90	38.80	4.40	1.18	0.13	0.10	0.10	0.04	0.32	0.01	2.13	1.39	0.11
LS-21	53.90	39.00	4.50	1.28	0.14	0.06	0.09	0.03	0.30	0.01	1.98	1.38	0.07
LS-22	54.00	38.60	4.10	1.61	0.11	0.14	0.08	0.06	0.30	0.01	1.93	1.40	0.15
LS-23	54.10	38.80	3.80	1.18	0.17	0.12	0.08	0.04	0.30	0.01	1.94	1.39	0.13
LS-24	53.90	40.20	4.30	1.47	0.15	0.07	0.10	0.03	0.27	0.01	1.84	1.34	0.08
LS-25	53.60	39.00	4.20	1.78	0.22	0.10	0.12	0.04	0.28	0.01	1.97	1.37	0.11
LS-26	53.40	38.80	4.20	1.89	0.08	0.33	0.09	0.10	0.28	0.01	1.64	1.38	0.34
LS-27	53.50	38.60	4.00	1.93	0.39	0.10	0.10	0.05	0.24	0.01	2.01	1.39	0.11
LS-28	53.40	38.70	4.20	2.75	0.14	0.42	0.13	0.14	0.28	0.02	1.64	1.38	0.44
LS-29	45.80	31.90	3.30	16.56	0.09	0.03	0.13	0.01	0.01	<0.01	2.85	1.44	<0.04
average value of LS-19–LS-28	53.77	38.94	4.21	1.59	0.19	0.15	0.10	0.06	0.29	0.01	1.93	1.43	0.16
average value of layer B	51.88	36.60	4.03	4.96	0.17	0.13	0.15	0.05	0.26	0.01	2.07	1.43	0.14

with an average of 53.74 wt %. Fluorine contents vary from 3.80 to 4.50 wt %, with an average of 4.19 wt %. SiO_2 contents range from 1.18 to 2.75 wt %, with an average of 1.67 wt %. Al_2O_3 contents vary from 0.07 to 0.42 wt %, with an average of

https://doi.org/10.1021/acsomega.3c06476
ACS Omega 2023, 8, 47938−47953

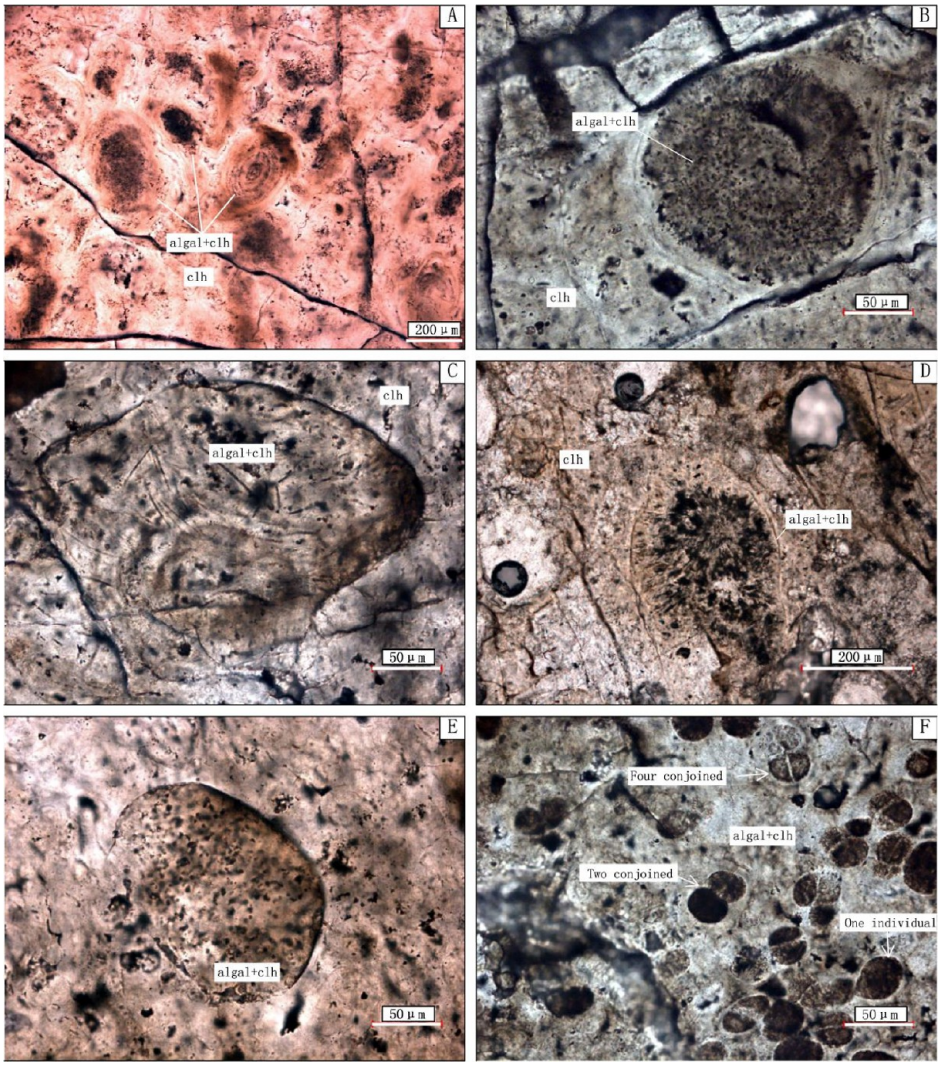

Figure 7. Microscopic features of the micritic phosphorite. (A) Concentric ring structure (sample B6; Dapingshan, Longshui). (B) Spherical structure containing abundant organic particles (sample B8; Dapingshan, Longshui). (C) Leaf-like structure containing filamentous organic matter (sample B8; Dapingshan, Longshui). (D) Spherical structure containing radiating organic matter (sample B9; Dapingshan, Longshui). (E) Egg-like structure containing abundant organic particles (sample B10; Dapingshan, Longshui). (F) Spherical structure containing groups of dark organic particles (sample B14; Dapingshan, Longshui). clh = collophanite; Qtz = quartz; Cln = chalcedony.

0.16 wt %. K_2O contents range from 0.03 to 0.14 wt %, with an average of 0.06 wt %. TiO_2 contents vary from 0.01 to 0.02 wt %, with an average of 0.01 wt %. Na_2O contents range from 0.24 to 0.32 wt %, with an average of 0.29 wt %. The average CaO/P_2O_5 ratio is 1.38, which is slightly higher than the theoretical value for apatite (1.35; Xu, 1977), indicating that there is a small amount of nonphosphatic CaO in the phosphorites.

P_2O_5 exhibits a significant positive correlation with CaO and F and a slightly negative correlation with MgO and SiO_2 (Table 2). The correlation coefficients (R) are as follows: P_2O_5−CaO = 0.73, P_2O_5−F = 0.60, P_2O_5−MgO = −0.65, and P_2O_5−SiO_2 = −0.73. In addition, the correlation coefficients of some major elements are as follows: CaO−F = 0.90, MgO−SiO_2 = 0.88, Al_2O_3−TiO_2 = 0.75, MgO−TiO_2 = 0.68, CaO−MgO = −0.89, F−MgO = −0.73, CaO−SiO_2 = −1.00, and F−SiO_2 = −0.91.

4.3. Trace Elements. Trace element data are given in Table 3. The Post-Archean Australian Shale (PAAS)-normalized trace element patterns are almost identical (Figure 9). All samples are enriched in Zn, Sr, U, Ba, and Pb, with enrichment coefficients ($\omega N/\omega N_{PAAS}$, N refers to some element) of 0.59−2.01 (average = 1.16), 2.46−3.20 (average = 2.69), 1.93−2.45 (average = 2.16), 0.24−0.43 (average = 0.35), and 0.11−0.22 (average = 0.16), respectively.

4.4. Rare-Earth Elements. Rare-earth element data are listed in Table 4. The ∑REE contents of the nodular phosphorite (LS18) and sandy phosphorite (LS29) are lower than those of micritic phosphorites, with values of 9.94 and 6.35 ppm. The ∑REE contents of the other samples vary from 36.99 to 56.82 ppm, with an average of 44.46 ppm. The overall mean ∑REE content is 38.41 ppm.

The δCe values of the samples vary from 0.52 to 0.72, with an average of 0.64. There are negative Ce and variable Eu anomalies. The Ce_{anom} values increase gradually from the bottom to the top of layer B, varying from −0.18 to −0.32, with an average of −0.24.

4.5. Carbon and Oxygen Isotopes. Micritic phosphorites were selected for stable C−O isotope analysis (Table 5). $\delta^{18}O$ values range from 13.76 to 16.13‰, with an average of

https://doi.org/10.1021/acsomega.3c06476
ACS Omega 2023, 8, 47938−47953

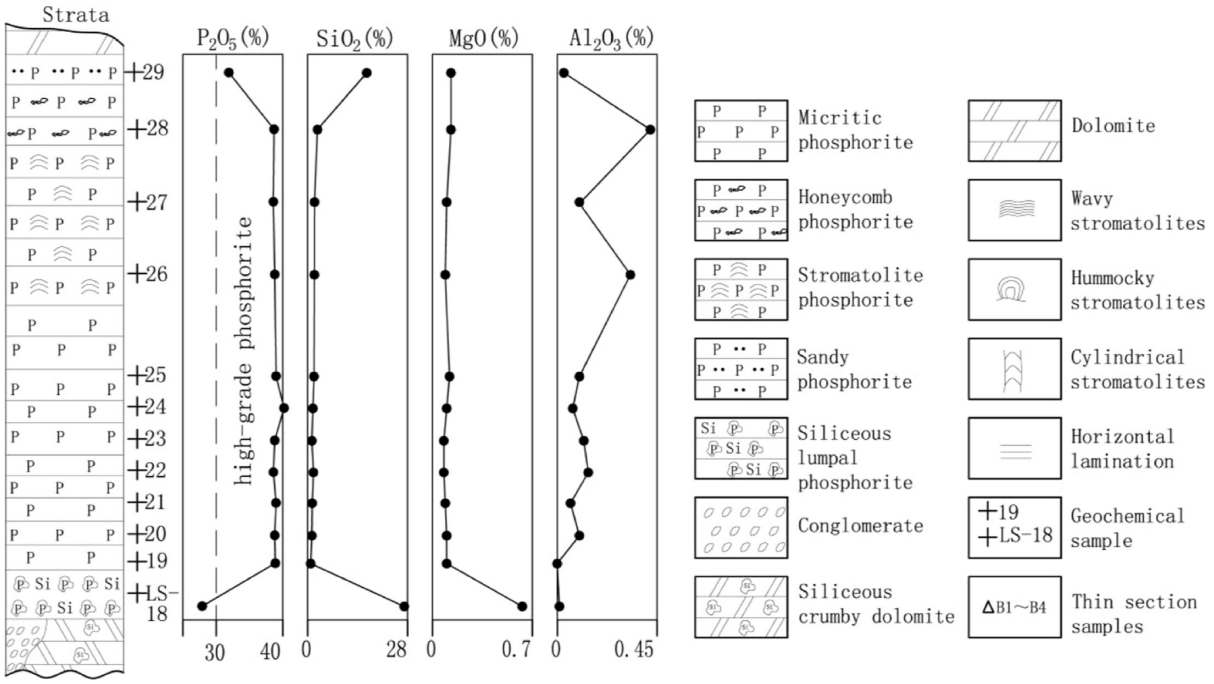

Figure 8. Stratigraphic variations of major elements in phosphorites from layer B.

Table 2. Correlations between Major Elements for Whole-Rock Samples of the Doushantuo Formation [$R > 0.5$ and $R < -0.5$ Represent Positive and Negative Correlations (Shown in Bold), Respectively; $-0.5 < R < 0.5$ Indicates No Correlation]

	CaO	P_2O_5	F	SiO_2	TFe_2O_3	Al_2O_3	MgO	TiO_2
CaO	1.00							
P_2O_5	**0.73**	1.00						
F	**0.90**	**0.60**	1.00					
SiO_2	**−1.00**	**−0.73**	**−0.91**	1.00				
TFe_2O_3	0.26	−0.14	0.22	−0.28	1.00			
Al_2O_3	0.20	0.42	0.10	−0.18	−0.20	1.00		
MgO	**−0.89**	**−0.65**	**−0.73**	**0.88**	−0.14	0.16	1.00	
TiO_2	−0.49	0.08	−0.02	**0.76**	−0.16	**0.75**	**0.68**	1.00

Table 3. Trace Element Data (Parts per Million) for Phosphorites in Layer B[a]

sampling sites	Co	Ni	V	Cr	Sr	Ba	Sb	Th	U	Cu	Mo	Pb	Zn	As
LS-18	0.6	<0.2	5	9	528	306	0.41	0.10	8.30	1.8	0.46	2.0	20	4.2
LS-19	1.0	4.6	7	13	586	274	0.81	0.24	7.58	3.3	0.47	4.3	93	5.6
LS-20	0.9	4.2	9	10	639	282	0.72	0.25	7.16	2.7	0.37	3.6	99	5.5
LS-21	0.8	3.7	9	9	565	197	0.79	0.29	6.93	2.1	0.36	3.0	91	5.2
LS-22	0.9	3.9	12	15	493	189	0.77	0.40	6.54	2.4	0.43	3.9	108	6.5
LS-23	0.9	3.4	10	12	491	159	0.82	0.32	7.07	2.2	0.51	3.6	80	5.9
LS-24	0.9	6.3	11	7	525	215	0.90	0.26	6.07	2.1	0.39	2.4	118	6.1
LS-25	0.9	3.4	8	8	599	280	0.66	0.32	5.98	1.9	0.35	2.1	68	4.6
LS-26	0.9	1.5	10	7	509	262	0.67	0.62	6.28	2.3	0.30	3.3	50	4.8
LS-27	0.9	5.6	8	7	456	179	1.16	0.40	6.32	2.6	0.26	2.1	112	5.4
LS-28	1.0	4.2	13	8	524	211	1.19	0.91	6.90	3.0	0.34	2.7	171	6.2
LS-29	0.9	21.7	19	5	47	31	1.10	0.06	0.63	2.9	0.27	1.1	540	2.6
average value	0.9	5.7	10	9	497	215	0.83	0.35	6.31	2.4	0.38	2.8	129	5.2
PAAS	23	55	150	110	200	650		14.6	3.1	50	1	20	85	
average value of $\omega N/\omega N_{PAAS}$	0.04	0.07	0.06	0.09	2.69	0.35		0.03	2.16	0.05		0.16	1.16	

[a]Notes: the PAAS normalization values were taken from Taylor and McLennan.[34]

14.60‰. $\delta^{13}C$ values vary from −15.79 to −8.70‰, with an average of −13.13‰.

A linear relationship between $\delta^{13}C_{V\text{-}PDB}$ and $\delta^{18}O_{V\text{-}PDB}$ can identify whether a sample has experienced diagenetic modification. There is no significant correlation between $\delta^{13}C_{V\text{-}PDB}$ and $\delta^{18}O_{V\text{-}PDB}$ values (Figure 10A), indicating that the samples were not affected by diagenesis. Manganese/Sr ratios can be used to evaluate late diagenetic changes as Sr loss

https://doi.org/10.1021/acsomega.3c06476
ACS Omega 2023, 8, 47938−47953

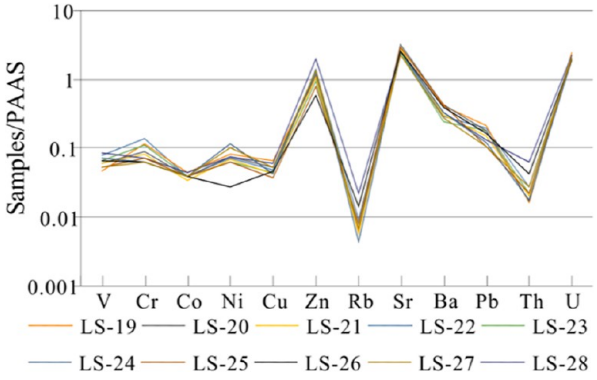

Figure 9. PAAS)-normalized trace element patterns of the phosphorites. The PAAS normalization values were taken from ref 34. Copyright 1985 Taylor and McLennan.

and Mn addition occur after sedimentation of marine authigenic rocks, especially when exposed to the meteoric water cycle.[37] It is generally thought that Mn/Sr < 10 is a threshold for the preservation of the primary stable C isotopic composition.[38] The Mn/Sr ratios of the studied samples are <10 (Table 5), and there is no significant correlation with P_2O_5 contents (Figure 10B), indicating that the samples were unaffected by diagenesis.

5. DISCUSSION

5.1. Origins of the Phosphorites. The microstructures in the nodular, micritic, stromatolitic, and honeycomb phosphorites are biological in origin. In particular, the oriented and unoriented spherical particles are fossils of benthic multicellular red algae. Such fossils have been reported from the Ediacaran Doushantuo period in central Guizhou.[39,40] Fossils of phosphatized algae with similar structures have also been found in the 1.6 Ga Chitrakote sedimentary rocks of central India.[41] The multicellular red algae fossils are well preserved, and there is no clastic material, which suggests that the algae were preserved in situ. The siliceous nodules are spheroidal or irregular in shape, with diameters of 0.3−2.0 cm, and they are either isolated or aggregated. The fine-grained, transparent, to dark spherules inside the nodules may be biological cells. These are surrounded by a phosphatic covering, which is rich in tiny spherules distributed in bundles (Figure 5B). There are also ctenocyst-like siliceous shells, indicating that these organisms had a certain ability to withstand wind and waves. Silica (i.e., quartz and chalcedony) infills between the aggregates and some quartz geodes are locally developed. These features are typical of a reef formed by algal organisms that became filled with siliceous materials.

The spherical particles are biogenic rather than clastic in origin. These particles can be cloud-shaped (Figure 4A), radiating (Figure 5B), leaf-shaped (Figure 5D), oval-shaped (Figure 5F), and fan-shaped (Figure 6F) and contain concentric rings (Figure 7A). The diameters vary from 0.05 to 2.00 mm, and the particles are poorly sorted. The interior of the particles contain fine spherical or filamentous material, which is mostly collophanite. These spherical particles are completely different from those in the sandy clastic phosphorites that are widely distributed in the Kaiyang area. The spherical particles in the sandy clastic phosphorites are well rounded and sorted, with diameters of 0.2−0.5 mm. There are many layers of fibrous apatite encrusted around these

Table 4. Rare-Earth Element Data (Parts per Million) for Phosphorites in Layer B[a]

sampling sites	La	Ce	Pr	Nd	Sm	Eu	Gd	Tb	Dy	Ho	Er	Tm	Yb	Lu	Y	ΣREE	Ce/Ce*	Eu/Eu*	Pr/Pr/*	Ce_{anom}	DyN/SmN
LS-18	2.0	2.60	0.44	2.1	0.51	0.14	0.69	0.10	0.60	0.12	0.34	0.04	0.23	0.03	5.9	9.94	0.60	1.08	1.11	−0.22	1.11
LS-19	6.7	10.60	1.96	9.9	2.50	0.61	2.82	0.46	2.71	0.53	1.43	0.17	0.91	0.12	23.8	41.42	0.65	1.06	1.05	−0.19	1.07
LS-20	6.4	10.00	1.88	9.3	2.29	0.55	2.54	0.39	2.38	0.46	1.25	0.14	0.77	0.11	20.2	38.46	0.68	1.06	1.05	−0.17	1.03
LS-21	6.2	10.10	1.88	9.3	2.21	0.50	2.30	0.35	1.99	0.41	1.11	0.13	0.64	0.09	17.0	37.21	0.70	1.03	1.05	−0.15	0.87
LS-22	7.9	12.35	2.40	11.8	2.77	0.61	2.88	0.45	2.59	0.54	1.44	0.17	0.85	0.11	22.3	46.86	0.67	1.00	1.06	−0.17	0.92
LS-23	7.2	11.20	2.18	10.7	2.57	0.56	2.71	0.41	2.54	0.53	1.36	0.16	0.81	0.11	21.2	43.04	0.64	1.00	1.09	−0.19	0.98
LS-24	7.6	9.24	2.13	10.2	2.32	0.53	2.70	0.37	2.20	0.45	1.11	0.12	0.68	0.08	18.2	39.73	0.55	0.98	1.14	−0.26	0.93
LS-25	8.9	10.20	2.40	11.3	2.52	0.55	2.51	0.39	2.27	0.43	1.11	0.13	0.72	0.09	18.5	43.52	0.52	1.03	1.17	−0.28	0.89
LS-26	13.7	16.40	2.89	12.6	2.92	0.98	3.83	0.52	3.14	0.61	1.62	0.19	0.99	0.13	25.5	60.52	0.61	1.35	1.14	−0.21	1.06
LS-27	7.1	8.81	2.00	9.4	2.11	0.48	2.45	0.34	2.02	0.39	1.04	0.14	0.63	0.08	15.9	36.99	0.52	0.97	1.18	−0.28	0.95
LS-28	10.1	14.15	3.00	14.4	3.46	0.80	3.77	0.55	3.20	0.60	1.52	0.17	0.97	0.13	24.3	56.82	0.60	1.03	1.13	−0.22	0.90
LS-29	1.3	1.90	0.30	1.4	0.27	0.09	0.40	0.06	0.28	0.06	0.17	0.02	0.09	0.01	3.0	6.35	0.67	1.14	1.00	−0.17	1.00

[a]Notes: $Ce/Ce^* = 2Ce_{SN}/(La_{SN} + Pr_{SN})$; $Eu/Eu^* = 2Eu_{SN}/(Sm_{SN} + Gd_{SN})$; $Pr/Pr^* = 2Pr_{SN}/(Ce_{SN} + Nd_{SN})$;[35] $Ce_{anom} = \log(3 \times Ce_N/[2 \times La_N + Nd_N])$.[34,36] SN = PAAS-normalized; N = NASC-normalized.

https://doi.org/10.1021/acsomega.3c06476
ACS Omega 2023, 8, 47938−47953

Table 5. Stable C−O Isotope Data for Phosphorites in Layer B

sampling sites	$\delta^{13}C_{V\text{-}PDB}$ (‰)	$\delta^{18}O_{V\text{-}PDB}$ (‰)	P_2O_5 (wt %)	CaO/P_2O_5	ωMn (ppm)	ωSr (ppm)	ωMn/ωSr
LS-19	−8.70	14.13	38.9	1.39	55	586	0.09
LS-20	−15.24	13.76	38.8	1.39	36	639	0.06
LS-21	−15.79	14.65	39.0	1.38	37	565	0.07
LS-22	−13.42	13.87	38.6	1.40	32	493	0.06
LS-23	−12.70	14.57	38.8	1.39	29	491	0.06
LS-24	−11.76	14.54	40.2	1.34	62	525	0.12
LS-25	−14.01	14.81	39.0	1.37	52	599	0.09
LS-26	−11.38	14.62	38.8	1.38	37	509	0.07
LS-27	−12.22	16.13	38.6	1.39	64	456	0.14
LS-28	−15.51	14.43	38.7	1.38	102	524	0.19
average value	−13.56	14.60	38.9	1.39			

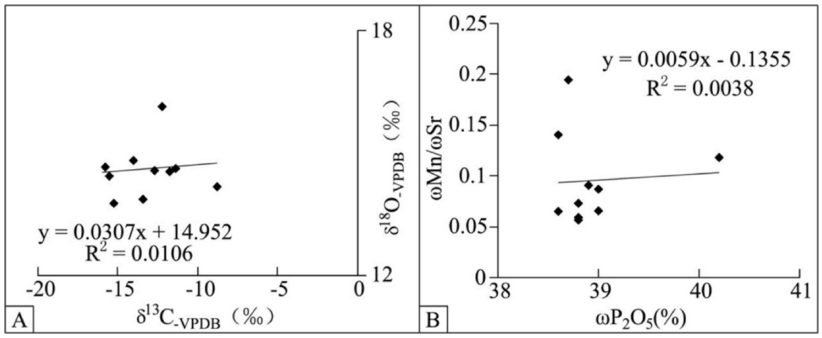

Figure 10. Plots of (A) $\delta^{13}C_{V\text{-}PDB}$ vs $\delta^{18}O_{V\text{-}PDB}$ and (B) Mn/Sr vs P_2O_5.

spherical particles,[42−44] and the internal structures and compositions of the particles are complex, with various forms of siliceous, clayey, and other clastic particles. The multicellular red algae fossils account for >70% of the fossil assemblage. This suggests that the studied phosphorites are biological phosphorites.

These phosphorites have pores along the bedding planes (Figure 3H). The bedding in the ore is poorly developed. In summary, layer B was a layered reef produced by reef-building organisms (i.e., mainly multicellular red algae). The wave resistance of the reef-building organisms created a suitable habitat for reef-dwelling organisms, and the interaction between reef-building and reef-dwelling organisms promoted rapid reef growth. The fossils of different types (Figures 4−7) in layer B at Longshui indicate that the biological diversity was relatively rich, significantly more so than in other sediments of the same age, which is also characteristic of a reef environment.[45] This indicates that the ore layer was originally an organic reef.

5.2. Depositional Environment of the Phosphorites. *5.2.1. Paleogeographic Setting.* The outcrop of layer B in the Doushantuo Formation at Longshui is a small and partially abandoned tidal channel deposit. The conglomerate (Figure 1E) at its base was formed by the high-energy water transport in the tidal channel. After the tidal channel was abandoned, bedded micritic phosphorite (Figure 1D) was deposited on the conglomerate. With further deposition of micritic phosphorite, the water became shallower, and stromatolites (Figure 1F) formed. During the vertical growth of the stromatolites, the individual columns became infilled with gravel. As the water became even shallower, honeycomb phosphorites (Figure 1H) formed. Therefore, it can be inferred that the outcrop represents a high-energy hydrodynamic setting of localized phosphatic accumulation in a beach environment.

5.2.2. Water Clarity. Aluminum and Ti are commonly used to determine the proportions of terrestrial detritus in authigenic sediments. In general, higher levels of Al and Ti indicate a greater proportion of terrestrial detritus, indicating a shallower water depth or a closer distance to the source.[46] The $\omega(Al_2O_3 + TiO_2)$ contents of the layer B ore vary from 0.02 to 0.44 wt %, which is the lowest content in the study area,[16,18,47] indicating that the water mass in the study area was far from the source and extremely clear, which would have been conducive to reef formation. Reefs are generally large in size, with extremely diverse and complex biological communities, and they have high productivity, which makes reefs one of the most productive biological communities in the ocean in terms of primary and secondary productivity and metabolic activity.[45]

5.2.3. Water Depth. The studied phosphorites are rich in many types of fossil organisms, particularly multicellular red algae. The presence of these algophytes in a primary, high-grade, micritic phosphorite suggests that phosphorite formation was closely related to the presence of red algae and that the breeding site of the red algae was favorable for phosphate crystallization. Studies of modern algae suggest that red algae inhabit mostly subtidal zones but can live at depths of 30−60 m below the low tide level in clear water or even on the seabed at a depth of 200 m.[48] Red algae are the main cementing organisms among the reef species in modern reefs, especially on the outer edge of the wave-affected reef.[45] This indicates that the phosphorites formed mainly at water depths of <200 m. The phosphate content depends on the growth density of the algae.

5.2.4. Redox Conditions. The geochemical properties of Ce are the same as those of the other lanthanides in anoxic seawater. In an oxic marine environment, soluble Ce^{3+} is oxidized to insoluble Ce^{4+} as CeO_2, which produces a large negative Ce anomaly in modern surface oxidizing waters.[49,50]

https://doi.org/10.1021/acsomega.3c06476
ACS Omega 2023, 8, 47938−47953

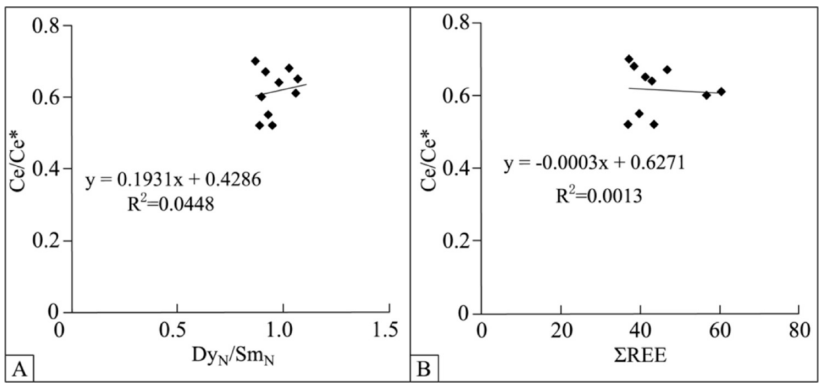

Figure 11. Plots of (A) Ce/Ce* vs ΣREE and (B) Ce/Ce* vs Dy_N/Sm_N.

Therefore, Ce anomalies can be used as a redox proxy.[51] McArthur and Walsh[52] suggested that negative Ce anomalies in seawater could be inherited by francolite formed under oxic seawater conditions. In general, Ce_{anom} < 0.1 represents oxic conditions, and Ce_{anom} > 0.1 represents anoxic conditions.[34,36]

Diagenesis can produce a negative correlation between Ce/Ce* and Dy_N/Sm_N values and a positive correlation between Ce/Ce* values and total REE contents.[51,53] The studied samples do not exhibit such correlations (Figure 11), suggesting that the Ce anomalies record the nature of the depositional environment during formation of the phosphorites.

Given that the sizes of the Ce anomalies can be overestimated owing to the high La concentrations,[35,53] it is necessary to further evaluate the actual Ce anomaly values. Because no chemical processes will result in Nd and Pr anomalies, actual Ce anomalies result in Pr/Pr* values that are not less <1.[35] Therefore, a plot of Pr/Pr* versus Ce/Ce* was used to assess the degree to which La affected the Ce anomaly values of the Longshui phosphorites (Figure 12). Most of the Ce anomalies are plotted in the IIIb field, which represents actual Ce anomalies (Figure 13A). Therefore, the Ce anomalies indicate the phosphorites formed in an oxic environment. The oxic depositional environment of layer B

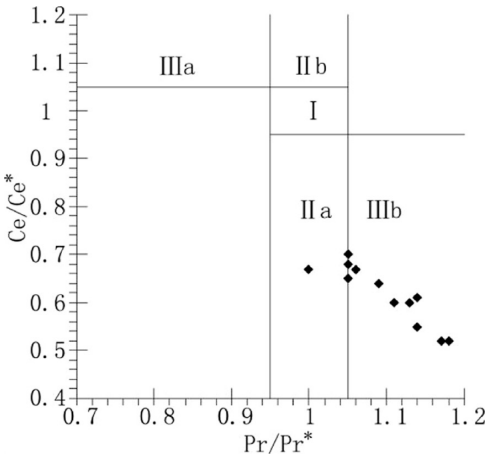

Figure 12. Plot of Pr/Pr* vs Ce/Ce*. Base map adapted with permission from ref35. Copyright 1996 Bau and Dulski. Domain I = no Ce and La anomalies; domain IIa = positive La and no Ce anomalies; domain IIIb = negative La and no Ce anomalies; domain IIIa = positive Ce anomalies; and domain IIIb = negative Ce anomalies.

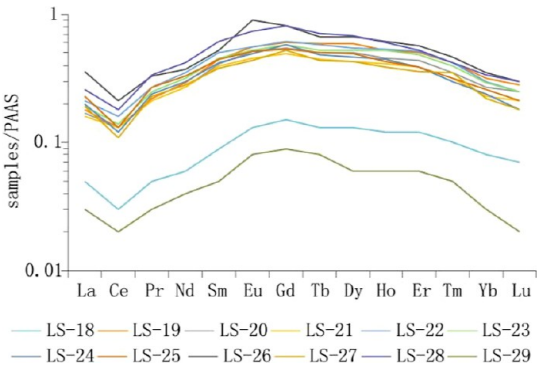

Figure 13. PAAS-normalized rare-earth element patterns for phosphorites in layer B at Longshui. PAAS normalizing values were taken from those of Taylor and McLennan (1985).

at Longshui is similar to that of layer B in the Weng'an phosphorite deposits.[18,54−56]

5.3. Biophosphorization. *5.3.1. Biological Fossils and Organic Matter in the Phosphorites.* Algal fossils account for >50% of the primary, high-grade, micritic phosphorites, which are generally leaf-like (Figure 6). Most of the fossils are completely preserved (Figures 4−6), indicating that they were preserved in situ. These organisms formed in an ecosystem with a high organic matter content and grew large organic structures by biomineralization. This indicates that the high-grade phosphorites were closely related to algal productivity.

5.3.2. Geochemical Evidence of Biophosphorization. Biogenic phosphorites, such as stromatolitic phosphorites, are characterized by low REE contents.[57] The REE contents of marine organisms are generally only a few parts per million, reflecting the low REE content of seawater.[58] Biogenic carbonate rocks also have low REE contents. The ΣREE contents of samples from the study area range from 6.35 to 56.82 ppm, with an average of 38.41 ppm, indicating the important role of organisms in the formation of the phosphorites. The REE patterns of the samples (Figure 13) are "hat-shaped", with middle REE enrichment and light−heavy REE depletion, similar to those of Wenlockian/Upper Cambrian phosphorites;[59] these features are consistent with those of almost all Phanerozoic phosphorites.[51] This also proves the biogenesis of phosphorites in the study area.

During the period of sediment burial, due to the oxidation of organic material and the reduction reaction of sulfate bacteria, the authigenic apatite contains obvious organic evolution carbon components, so its isotopic composition is charac-

https://doi.org/10.1021/acsomega.3c06476
ACS Omega 2023, 8, 47938−47953

terized by enrichment of light carbon.[60] The $\delta^{13}C$ values of the studied samples range from −15.79 to −8.70‰, with an average of −13.13‰—much lower than those of layer A (−2.01‰) and layer B (−3.25‰) in the Weng'an phosphorite deposits,[7] apatite from central Guizhou (−3.63‰ to +0.10‰),[60] modern marine carbonates (0‰ ± 4‰), and authigenic phosphorites from the Namibian continental shelf (−3.31‰).[61] This indicates that the sample has CO_2 from decomposition of microorganisms and organic matter, and the micrite phosphorite in layer B was biogenic phosphorite. The average $\delta^{18}O$ value of the studied samples is 14.60‰, which is much higher than those of layer A (−7.55‰) and layer B (−5.02‰) in the Weng'an phosphorite deposits[7] and lower than those for modern marine apatite (19−26‰) and is related to the biological productivity.[62] The high $\delta^{18}O_P$ value of modern marine apatite is related to the strong biological processes in the ocean, while the low $\delta^{18}O_P$ value of apatite in igneous rocks and meteorites is about 6−8‰ because there is little biotransformation in igneous rocks and meteorites. The very low $\delta^{13}C$ values and high $\delta^{18}O$ values of the samples indicate that the phosphorites in layer B are microbial phosphorites from a highly bioproductive environment affecting the isotope system.

The cell walls of algae consist primarily of polysaccharides, proteins, and lipids, which form a viscous, negatively charged structure with functional groups that can bind to ions. Algal membranes are selectively permeable, enabling the concentration of various ions.[63] In terms of their affinity for common ions, algae tend to preferentially enrich elements such as Pb, Fe, Cu, Zn, Mn, Mo, Sr, Ni, V, Se, As, and Co (in descending order).[64] The samples analyzed in this study exhibit enrichments in elements such as Zn, Sr, U, Ba, and Pb (Figure 9), similar to phosphorite deposits found in other regions of Guizhou Province that have been affected by bacterial and algal activity.[19,65,66] As such, the formation of phosphorites in the study area can be attributed to the biological activity of these microorganisms.

5.3.3. Biological Contribution to Phosphogenesis. The studied phosphorites are the products of initial phosphogenesis, and they are rich in various algal fossils. The stromatolites were also formed by algal trapping. The clastic phosphorites that are widely distributed in the Kaiyang area have undergone fragmentation, transport, and redeposition,[30,44,67] and a large amount of organic matter and biological fossils/fragments are retained in the phosphate particles.[11,32,68,69] Biological processes play an important role in controlling the formation of high-grade phosphorites in this area.

Organisms consist of organic matter, including carbohydrates, free and bonded lipids, organic C, and humic acids.[70] The phosphorites in the study area contain a plethora of phosphatized bacterial and algal fossils, and no fossils of organisms that have not been (partially) phosphatized have been found. However, it cannot be determined whether these organisms were initially phosphatized. Almost all of these fossils, whether algal or animal in origin,[71,72] were preserved by undifferentiated phosphorylation. This phosphorylation contributed significantly to the formation of thick and high-grade phosphorites. The development of the initial reef phosphorites had a controlling effect on the phosphorite grade.

The enrichment of P by algae is driven mainly by the following four processes. First, algal cells can directly absorb P from the environment in the form of orthophosphate (HPO^{4-}) and utilize organic phosphate through phosphatase activity.[73] Modern blue−green algae, such as spirulina, can rapidly absorb P from a P-rich environment by synthesizing polyphosphates.[74] Polyphosphates enriched in algal cells can directly form minerals dominated by carbonate fluorophosphate under normal temperature and pressure and slightly alkaline conditions in the Ca^{2+}−HPO_4^{2-}−HCO^{3-}−F^-−H_2O system. Second, algae can mechanically capture and enrich P. There are two types of phosphatized algal fossils in layer B at Longshui, which are the phosphate crystal conglomerates and silica grain-like phosphate conglomerates. The phosphate crystal conglomerates contain a large amount of fossils, mainly red algae, and most have not undergone mechanical fragmentation. The silica grain-like phosphate conglomerates formed by the in situ transformation of red algal fossils into phosphates in siliceous rocks. Similar phosphate conglomerates containing algal fossils also occur at Weng'an in Guizhou Province[39,69] and at Jingxiang in Hubei Province.[75] Phosphorus-rich layered rocks formed by the capture of algae are also abundant in various phosphate deposits.[76−78] Third, algae can modify the sedimentary environment and promote the deposition of phosphates. Algal photosynthesis relies on the consumption of CO_2 in water, which changes the water pH. When the pH reaches 8.0 ± 0.5, dissolved phosphates will crystallize in large quantities.[4,79] Fourth, the decomposition of algae increases the concentration of P in the environment. During the decomposition and transformation of the algae or other organic components (e.g., proteins, lipids, and carbohydrates), amino acids, sugars, CH_4, CO_2, and P in the form of HPO^{4-} are released to water. If algae continue to grow, reproduce, die, and decompose, then a large amount of P will accumulate in water. These four factors led to the formation of high-grade sedimentary phosphorites in the study area.

6. CONCLUSIONS

The origins of phosphorites in Guizhou Province are controversial because most of the ores in the Kaiyang phosphate ore deposit are recycled phosphorites. Based on the results of a sedimentological, petrological, geochemical, and isotope study of layer B at Longshui Kaiyang, we propose that the ore deposit was a reef formed mainly by red algae. The reef was layered and developed in a small abandoned tidal channel, and its sedimentary environment was characterized by clear and oxidized seawater. The discovery of this high-grade protist phosphorite shows that the involvement of algae was key to the formation of the Kaiyang phosphate-rich deposit.

The studied phosphorite deposits provide new insights into the initial phosphogenesis of high-grade phosphate-rich ores and are an important basis for mineralization models of phosphate-rich deposits. However, owing to the limited scale of the present study, the paleogeography and sedimentary environment need to be further studied over a wider area.

AUTHOR INFORMATION

Corresponding Author

Ruidong Yang − *College of Resource and Environmental Engineering, Guizhou University, Guiyang 550025, China; Key Laboratory of Karst Georesources and Environment, Ministry of Education, Guizhou University, Guiyang 550025 Guizhou, P. R. China*; Email: rdyang@gzu.edu.cn

https://doi.org/10.1021/acsomega.3c06476
ACS Omega 2023, 8, 47938−47953

Authors

Wenming Wu − *College of Resource and Environmental Engineering, Guizhou University, Guiyang 550025, China; Geological Brigade 105, Bureau of Geology and Mineral Exploration and Development of Guizhou Province, Guiyang 550018, China; Innovation Center of Ore Resources Exploration Technology in the Region of Bedrock, Ministry of Natural Resources of People's Republic of China, Guiyang 550081, China;* orcid.org/0000-0003-1684-6863

Jianzhong Liu − *Innovation Center of Ore Resources Exploration Technology in the Region of Bedrock, Ministry of Natural Resources of People's Republic of China, Guiyang 550081, China; Bureau of Geology and Mineral Exploration and Development of Guizhou Province, Guiyang 550004, China*

Zepeng Wang − *Geological Brigade 105, Bureau of Geology and Mineral Exploration and Development of Guizhou Province, Guiyang 550018, China; Innovation Center of Ore Resources Exploration Technology in the Region of Bedrock, Ministry of Natural Resources of People's Republic of China, Guiyang 550081, China*

Shaohu Li − *State Key Laboratory of Biogeology and Environmental Geology & School of Earth Sciences, China University of Geosciences, Wuhan 430074, China*

Yunbin Shao − *Geological Brigade 105, Bureau of Geology and Mineral Exploration and Development of Guizhou Province, Guiyang 550018, China*

Yamei Deng − *Geological Brigade 105, Bureau of Geology and Mineral Exploration and Development of Guizhou Province, Guiyang 550018, China*

Taiping Ye − *Innovation Center of Ore Resources Exploration Technology in the Region of Bedrock, Ministry of Natural Resources of People's Republic of China, Guiyang 550081, China; Guizhou Central Laboratory of Geology and Mineral Resources, Bureau of Geology and Mineral Exploration and Development of Guizhou Province, Guiyang 550018, China*

Chaokun Luo − *College of Resource and Environmental Engineering, Guizhou University, Guiyang 550025, China*

Lei Gao − *College of Resource and Environmental Engineering, Guizhou University, Guiyang 550025, China*

Jiyan Chen − *College of Resource and Environmental Engineering, Guizhou University, Guiyang 550025, China*

Haili Ren − *College of Resource and Environmental Engineering, Guizhou University, Guiyang 550025, China*

Chengfu Yang − *Geological Brigade 105, Bureau of Geology and Mineral Exploration and Development of Guizhou Province, Guiyang 550018, China; Innovation Center of Ore Resources Exploration Technology in the Region of Bedrock, Ministry of Natural Resources of People's Republic of China, Guiyang 550081, China*

Junhai Li − *Geological Brigade 105, Bureau of Geology and Mineral Exploration and Development of Guizhou Province, Guiyang 550018, China; Innovation Center of Ore Resources Exploration Technology in the Region of Bedrock, Ministry of Natural Resources of People's Republic of China, Guiyang 550081, China*

Daxue Wan − *Geological Brigade 105, Bureau of Geology and Mineral Exploration and Development of Guizhou Province, Guiyang 550018, China*

Wenxing Tai − *Geological Brigade 105, Bureau of Geology and Mineral Exploration and Development of Guizhou Province, Guiyang 550018, China*

Complete contact information is available at: https://pubs.acs.org/10.1021/acsomega.3c06476

Notes

The authors declare no competing financial interest.

■ ACKNOWLEDGMENTS

This study was funded by the National Natural Science Foundation of China (Grants U1812402, 41890841, and 51164004), the Science and Technology Planning Project of Guizhou Province (no. [2022] ZD003 and no. CXTD[2021] 007), and the Project of Bureau of Geology and Mineral Exploration and Development of Guizhou Province [2023] TD003.

■ REFERENCES

(1) Chen, D. F.; Dong, W. Q.; Zhu, B. Q.; Chen, X. P. Pb-Pb ages of Neoproterozoic Doushantuo phosphorites in South China: constraints on early metazoan evolution and glaciation events. *Precambrian Res.* **2004**, *132*, 123−132.

(2) Zhang, S. H.; Jiang, G. Q.; Zhang, J. M.; Song, B.; Kennedy, M. J.; Christie-Blick, N. U-Pb sensitive high-resolution ion microprobe ages from the Doushantuo Formation in south China: Constraints on late Neoproterozoic glaciations. *Geology* **2005**, *33*, 473−476.

(3) Yin, C. Y.; Tang, F.; Liu, Y. O.; Gao, L. Z.; Yang, Z. O.; Wang, Z. O.; Liu, P. J.; Xing, Y. S.; Song, B. New U-Pb zircon ages from the Ediacaran (Sinian) System in the Yangtze Gorges: Constraint on the age of Miaohe biota and Marinoan glaciation. *Geol. Bull. China* **2005**, *24*, 393−400.

(4) Zhu, S. X.; Wang, Y. G. *Phosphatic stromatolites in Kaiyang phosphorite deposits*; Geological Publishing House: Guizhou, China. Beijing, 1982, pp 143−153.

(5) Zhu, S. X.; Wang, Y. G. Discussion on the genesis of Kaiyang phosphate deposit. *Chin. Sci. Bull.* **1983**, *28* (19), 1191−1194.

(6) Du, Y. S.; Zhang, G. Y.; Chen, G. Y.; Liu, J. Z.; Wang, Z. P.; Xu, Y. Y. *Three sedimentary and metallogenic stages of phosphate-rich ore: a new understanding of the mineralization mechanism of phosphate-rich ore in Kaiyang, Guizhou. China. Jiaozuo* 2016; pp 175−176.

(7) Zhang, Y. G.; Pufahl, P. K.; Du, Y. S.; Chen, G. Y.; Liu, J. Z.; Chen, Q. G.; Wang, Z. P.; Yu, W. C. Economic phosphorite from the Ediacaran Doushantuo Formation, South China, and the Neoproterozoic-Cambrian Phosphogenic Event. *Sediment. Geol.* **2019**, *388*, 1−19.

(8) Liu, J. Z.; Wang, Z. P.; Du, Y. S.; Zhang, Y. G.; Wu, W. M.; Chen, G. Y.; Fu, Z. K.; Wan, D. X.; Wang, D. F.; Tan, D. W. Enrichment mechanism of phosphorite deposits and significant breakthrough in "Triunity Model" for ore prospecting in the Ediacaran Doushantuo Formation of eastern Kaiyang region. *J. Palaeogeogr.* **2020**, *22* (05), 913−928.

(9) Yuan, X. L. A review of studies on a neoproterozoic microfossil assemblage: Weng'an biota at Weng'an, Guizhou, SW China. *Acta Micropalaeontologica Sinica.* **1999**, *16* (03), 281−286.

(10) Liu, P. J.; Xiao, S. H.; Yin, C. Y.; Chen, S. M.; Zhou, C. M.; Li, M. Ediacaran acanthomorphic Acritarchs and other microfossils from Chert Nodules of the Upper Doushantuo Formation in the Yangtze Gorges Area, South China. *J. Paleontol.* **2014**, *88*, 1−139.

(11) Dongxu, Z. Enrichment of phosphorus by algae. *Adv. Earth Sci.* **1990**, *5* (03), 15−18.

(12) Zhang, J.; Yuan, X. L. Discovery of the sexual reproductive structure of multicellular red algae at the end of the Proterozoic. *Sci. China, Ser. B: Chem.* **1995**, *25* (07), 749−754.

(13) Chen, M. E.; Xiao, Z. Z.; Yuan, X. L. A new assemblage of megafossils—miaohe biota from upper Sinian Doushantuo Formation, Yangtze Gorges. *Acta Palaeontol. Sin.* **1994**, *33*, 391−403.

(14) Xiao, S. H.; Zhang, Y.; Knoll, A. H. Three-dimensional preservation of algae and animal embryos in a Neoproterozoic phosphorite. *Nature* **1998**, *391*, 553−558.

(15) Guo, Q. J.; Yang, W. D.; Liu, C. Q.; Strauss, H.; Wang, X. L.; Zhao, Y. L. Sedimentary Geochemistry Research on the Radiation of Weng' an Biota and the Formation of the Phosphorite Ore Deposit, Guizhou. *Bull. Mineral., Petrol. Geochem.* **2003**, *22* (03), 202−208.
(16) Deng, K. Y.; Wu, B.; Luo, M. X.; Luo, C.; Long, J. X. Phosphate rock geochemistry of the Doushantuo Formation in Shuangshanping, Kaiyang of Guizhou Province and its genetic significance. *J. Geol.* **2015**, *51* (01), 123−132.
(17) Chen, Q. Y.; Chen, M. E.; Li, J. Y. Microbial-organic effects on formation of the sedimentary apatite. *Sci. Geol. Sin.* **2000**, *35* (03), 316−324.
(18) Yang, H. Y.; Xiao, J. F.; Xia, Y.; Xie, Z. J.; Tan, Q. P.; Xu, J. B.; Guo, H. Y.; He, S.; Wu, S. W. Origin of the Ediacaran Weng'an and Kaiyang phosphorite deposits in the Nanhua basin, SW China. *J. Asian Earth Sci.* **2019**, *182*, 103931.
(19) Yang, H. Y.; Xiao, J. F.; Hu, R. Z.; Xia, Y.; He, H. X. Formation environment and metallogenic mechanism of Weng'an Phosphorite in the Early Sinian. *J. Palaeogeogr.* **2020**, *22* (05), 929−946.
(20) Zhang, Y. G.; Du, Y. S.; Liu, J. Z.; Wang, Z. P.; Deng, C. Phospho genesis of Ediacaran phosphorite from the Doushantuo Formation in Guizhou Province and its coupling relation with the Neoproterozoic Oxygenation Even. *J. Palaeogeography (Chinese edition)* **2020**, *22*, 893−912.
(21) Föllmi, K. B.; Garrison, R. E.; Grimm, K. A. *Stratification in phosphatic sediments: illustrations from the Neogene of Central California*; Springer-Verlag: Heidelberg, 1991.
(22) Wang, J.; Li, Z. History of Neoproterozoic rift basins in South China: implications for Rodinia break-up. *Precambrian Res.* **2003**, *122*, 141−158.
(23) Wang, J.; Zeng, Z. G.; Chen, W. X.; Wang, Z. J.; Xiong, G. Q.; Wang, X. H. The Neoproterozoic rift systems in southern China: New evidence for the sedimentary onlap and its initial age. *Sediment. Geol. Tethyan Geol.* **2006**, *26*, 7.
(24) Jiang, G. Q.; Shi, X. Y.; Zhang, S. H.; Wang, Y.; Xiao, S. H. Stratigraphy and paleogeography of the Ediacaran Doushantuo Formation (ca. 635−551Ma) in South China. *Gondwana Res.* **2011**, *19*, 831−849.
(25) Jiang, W. Z.; Jian, W.; Wen, Z. J.; Ping, Y.; Hong, L. J.; Ke, X. S. Crust Extensional Activity during the Transition from Sinian-(Ediacaran) to Cambrian in Yangtze Block: Evidences from the Depositional Sequence and Its Geochemical Data. *Geol. Rev.* **2011**, *57*, 731−742.
(26) Wang, J.; Duan, T. Z.; Xie, Y.; Wang, Z. J.; Hao, M.; Liu, W. The tectonic evolution and its oil and gas prospect of southeast margin of Yangtze Block. *Geol. Bull. China* **2012**, *31* (11), 1739−1749.
(27) Vernhet, E. Paleobathymetric influence on the development of the late Ediacaran Yangtze platform (Hubei, Hunan, and Guizhou provinces, China). *Sediment. Geol.* **2007**, *197*, 29−46.
(28) Zhou, C.; Xiao, S. Ediacaran δ13C chemostratigraphy of South China. *Chem. Geol.* **2007**, *237*, 89−108.
(29) Zhu, M.; Zhang, J.; Yang, A. Integrated Ediacaran (Sinian) chronostratigraphy of South China. *Palaeogeogr., Palaeoclimatol., Palaeoecol.* **2007**, *254*, 7−61.
(30) Ye, L. J.; Chen, Q. Y.; Liu, K. W. Physical enrichment—a new theory on the genesis of industrial phosphorite deposits. *Acta Sedimentol. Sin.* **1986**, *4* (03), 1−22.
(31) Zhou, C. M.; Xue, Y. S.; Zhang, J. M. Stratigraphyand Sedimentary Environment of the Upper Sinian Doushantuo Formation In Weng'an Phosphorite Deposit, Guizhou Province. *J. Stratigraphy* **1998**, *22*, 70−76.
(32) Wu, W. M.; Yang, R. D.; Liu, J. Z.; Wang, Z. P.; Luo, C. K.; Ye, T. P.; Feng, K. N.; Yang, G. H.; Wang, L. B.; Liu, S.; Wang, D. F.; Huang, Y.; Pan, Q. Q.; Zhang, C. Sedimentary characteristics and biophosphorization of the Sinian Yangshui Formation in Longshui, Kaiyang, Guizhou Province. *J. Palaeogeogr.* **2021**, *23* (03), 625−638.
(33) Chen, G. Y.; Du, Y. S.; Zhang, Y. G.; Chen, Q. G.; Fan, Y. M.; Wang, Z. P.; Tan, H. Spatial and temporal variation and mineralization model of the Sinian phosphorites-bearing sequences in central Guizhou Province. *Geol. Sci. Technol. Inf.* **2015**, *34* (06), 17−25.
(34) Taylor, S. R.; Mclennan, S. M. *The Continental Crust: its Composition and Evolution: An Examination of the Geochemical Record Preserved in Sedimentary Rocks*; Blackwell Scientific Publications: Oxford, 1985.
(35) Bau, M.; Dulski, P. Distribution of yttrium and rare-earth elements in the Penge and Kuruman iron-formations, Transvaal Supergroup, South Africa. *Precambrian Res.* **1996**, *79*, 37−55.
(36) Haskin, L. A.; Wildeman, T. R.; Haskin, M. A. An accurate procedure for the determination of the rare earths by neutron activation. *J. Radioanal. Chem.* **1968**, *1*, 337−348.
(37) Veizer, J.; Ala, D.; Azmy, K.; Bruckschen, P.; Buhl, D.; Bruhn, F.; Carden, G. A. F.; Diener, A.; Ebneth, S.; Godderis, Y.; et al. 87Sr/86Sr, δ13C and δ18O evolution of Phanerozoic seawater. *Chem. Geol.* **1999**, *161*, 59−88.
(38) Kaufman, A. J.; Knoll, A. H. Neoproterozoic variations in the C-isotopic composition of seawater: stratigraphic and biogeochemical implications. *Precambrian Res.* **1995**, *73*, 27−49.
(39) Zhao, D. X. The discovery of phosphatic red algae in the Sinian Doushantuo Formation. *Acta Sedimentol. Sin.* **1986**, *04* (01), 126−127.
(40) Yun, Z. Multicellular thallophytes with differentiated tissues from Late Proterozoic phosphate rocks of South China. *Lethaia* **1989**, *22*, 113−132.
(41) Bengtson, S.; Sallstedt, T.; Belivanova, V.; Whitehouse, M. Three-dimensional preservation of cellular and subcellular structures suggests 1.6 billion-year-old crown-group red algae. *PLoS Biol.* **2017**, *15*, No. e2000735.
(42) Dongye; Ji, Q. Z.; Wang, S. H. The Discovery of the trace fossils of microbes in the rocks of Sinian Doushantou Formation Southwest China. **1984**, 346−348.
(43) Wu, W. M.; Yang, R. D.; Xu, S. L.; Ren, H. L.; Liu, J. Z.; Wang, Z. P.; Wang, D.; Tan, D. W.; Li, L. Analysis of enrichment factors for super-large phosphate deposit in Doushantuo Formation in Kaiyang, Guizhou. *Industrlal Minerals & Processing*, 2017; pp 33−37.
(44) Zhang, Y. G.; Du, Y. S.; Chen, G. Y.; Liu, J. Z.; Chen, Q. G.; Zhao, Z.; Wang, Z. P.; Deng, C. Three stages dynamic mineralization model of the phosphate-rich deposits: Mineralization mechanism of the Kaiyang-type high-grade phosphorite in central Guizhou Province. *J. Palaeogeogr.* **2019**, *21* (02), 351−368.
(45) Kuznecov, B. *Reef geology and oil−gas property of reefs*; Petroleum Industry Press: Beijing, 1983.
(46) Zhu, X. K.; Peng, Q. Y.; Zhang, R. B.; An, Z. Z.; Zhang, F. F.; Yan, B.; Li, J.; Gao, Z. F.; Tan, Y. Geological and Geochemical Characteristics of the Daotuo Super-Large Manganese Ore Deposit at Songtao Country in Guizhou Province. *Acta Geologica Sinica.* **2013**, *87* (09), 1335−1348.
(47) Xiao, Y. *The geochemistry and sediment environment of phosphate deposits in Sinian system, Guizhou province*. Ph.D thesis; China University of Geosciences: China, Beijing, 2010;.
(48) Qian, S. B.; Liu, D. Y.; Sun, J. *Marine Phycology*; China Ocean University Press: Qingdao, 2005.
(49) Holser, W. T. Evaluation of the application of rare-earth elements to paleoceanography. *Palaeogeogr., Palaeoclimatol., Palaeoecol.* **1997**, *132*, 309−323.
(50) Pourret, O.; Davranche, M.; Gruau, G.; Dia, A. New insights into cerium anomalies in organic-rich alkaline waters. *Chem. Geol.* **2008**, *251*, 120−127.
(51) Shields, G.; Stille, P. Diagenetic constraints on the use of cerium anomalies as palaeoseawater redox proxies: an isotopic and REE study of Cambrian phosphorites. *Chem. Geol.* **2001**, *175*, 29−48.
(52) Mcarthur, J. M.; Walsh, J. N. Rare-earth geochemistry of phosphorites. *Chem. Geol.* **1984**, *47*, 191−220.
(53) Morad, S.; Felitsyn, S. Identification of primary Ce-anomaly signatures in fossil biogenic apatite: implication for the Cambrian oceanic anoxia and phosphogenesis. *Sediment. Geol.* **2001**, *143*, 259−264.

https://doi.org/10.1021/acsomega.3c06476
ACS Omega 2023, 8, 47938−47953

(54) Chen, D. F.; Dong, W. Q.; Qi, L.; Chen, G. Q.; Chen, X. P. Possible REE constraints on the depositional and diagenetic environment of Doushantuo Formation phosphorites containing the earliest metazoan fauna. *Chem. Geol.* **2003**, *201* (1−2), 103−118.
(55) Xie, Q. L.; Chen, D. F.; Qi, L.; Chen, X. P. Ree geochemistry of doushantuo phosphorites and paleoenvironmental changes in weng'an area, south China. *Acta Mineral. Sin.* **2003**, *23* (04), 289−295.
(56) Wu, K.; Ma, D. S.; Pan, J. Y.; Nie, W. M.; Zhou, J.; Xia, F.; Liu, L. The geochemistry of phosphorite of Doushantuo Formation in Weng'an, China: insights from trace elements and REE. *J. East China Inst. Chem. Technol.* **2006**, *29* (02), 108−114.
(57) Zheng, W. Z.; Dongye, M. X.; Hu, L. L. Ree geochemistry of phosphorites of the Sinian Doushantou Formation in Western Hubei. *Geol. Rev.* **1992**, *38* (04), 352−359.
(58) Wang, Z. G.; Yu, X. Y.; Zhao, Z. H. *Geochemistry of rare earth elements*; Science Press: Beijing, China, 1989; pp 292−320.
(59) Ilyin, A. V. Rare-earth geochemistry of old' phosphorites and probability of syngenetic precipitation and accumulation of phosphate1In memory of Richard P. Sheldon1. *Chem. Geol.* **1998**, *144*, 243−256.
(60) Chen, Q. Y.; Feng, L. Y. Sulphur and Carbon Isotopes of Sedimentary Apatite, Guizhou Province and Their Geological Significance. *Acta Petrol. Sin.* **1996**, *12* (04), 97−100.
(61) Burnett, W. C. Geochemistry and origin of phosphorite deposits from off Peru and Chile. *Geol. Soc. Am. Bull.* **1977**, *88*, 813−823.
(62) Blake, R. E.; Chang, S. J.; Lepland, A. Phosphate oxygen isotopic evidence for a temperate and biologically active Archaean ocean. *Nature* **2010**, *464*, 1029−1032.
(63) Crist, R. H.; Oberholser, K.; Shank, N.; Nguyen, M. Nature of bonding between metallic ions and algal cell walls. *Environ. Sci. Technol.* **1981**, *15*, 1212−1217.
(64) Mahan, C. A.; Majidi, V.; Holcombe, J. A. Evaluation of the metal uptake of several algae strains in a multicomponent matrix utilizing inductively coupled plasma emission spectrometry. *Anal. Chem.* **1989**, *61*, 624−627.
(65) Mi, W. T.; Li, D. L.; Feng, Z. Q.; Wu, X. C.; Niu, X. Research on the geochemical characteristics of phosphorites of Doushantuo Formation in Wong'an county, Guizhou. *Contrib. Geol. Miner. Resour. Res.***2013**, *28*, 101−105.
(66) Dongye, M. X. *Ore-forming theory and practice of phosphorite*; Geological Publishing House: Beijing, 2015.
(67) Zhang, Y. G. *Sedimentary Geology of the Phosphorite deposits and Phosphogenic Event from Ediacaran Doushantuo Formation in Central Guizhou Provinve*. Ph.D thesis; China University of Geosciences: China, Wuhan, 2019;.
(68) Dongye, M. X. Phosphorites formed by the action of microorganism. *Acta Sedimentol. Sin.* **1985**, *3* (03), 1−6.
(69) Zhou, C. M.; Xue, Y. S. Rhodolith-like grain deposit from the neoproterozoic Doushantuo Formation in Weng'an, Guizhou, China. *Acta Micropalaeontologica Sinica.* **1999**, *16* (03), 275−280.
(70) Baturin, G. N. The Origin of Marine Phosphorites. *Int. Geol. Rev.* **1989**, *31*, 327−342.
(71) Xiao, S.; Knoll, A. H. Fossil preservation in the Neoproterozoic Doushantuo phosphorite Lagerstatte, South China. *Lethaia* **1999**, *32*, 219−240.
(72) Xue, Y. S.; Zhou, C. M.; Tang, T. F. Animal Embryos", a misinterpretation of Neoproterozoic microfossils. *Acta Micropalaeontologica Sinica.* **1999**, *16* (01), 5−8.
(73) Riley, J. P.; Skirrow, G. *Chemical Oceanography*; Ocean Press: Beijing, 1982.
(74) Liu, Z. L.; Liu, X. X.; Wang, Y. J. Accumulation of phosphorus and mineralizational significance of algal cells. *Acta Bot. Sin.* **1994**, *36* (12), 957−962.
(75) Zhou, C. M.; Yuan, X. L.; Xiao, S. H.; Chen, Z.; Xue, Y. S. Phosphatized fossil assemblage from the Doushantuo Formation in Baokang, Hubei province. *Acta Micropalaeontologica Sinica.* **2004**, *21* (04), 349−366.
(76) Xia, W. J.; Yin, J. C.; Li, X. H.; Zhang, T. G. An approach to the origin and features of late Sinian phosphatic stromtolites. *Acta Geologica Sinica.* **1987**, 82−90.
(77) Cao, R. J. Phosphatic stromatolite b1oherms and associated microlbial fossils from the Sinian Doushantuo format1on central Guizhou, South China. *Acta Palaeontol. Sin.* **1997**, *36* (03), 27−30.
(78) Zhang, W.; Yang, R. D.; Mao, T.; Ren, H. L.; Gao, J. B.; Chen, J. Y. Sedimentary environment and mineralization mechanism of the Stromatolitic Phosphorite in the Ediacaran Dengying Formation, Weng'an County of Guizhou Province, China. *Geol. J. China Univ.* **2015**, *21* (02), 186−195.
(79) Sheng, Z. Q. A study on origin of phosphatic stromatolite. *Acta Geologica Sinica.* **1984**, No. 03, 214−221.

https://doi.org/10.1021/acsomega.3c06476
ACS Omega 2023, 8, 47938−47953